# Elastic constants of hcp $^4$He: Path-integral Monte Carlo results versus experiment

Luis Aldemar Peña Ardila, Silvio A. Vitiello, and Maurice de Koning*

*Instituto de Física Gleb Wataghin, Universidade Estadual de Campinas, UNICAMP, 13083-859, Campinas, São Paulo, Brazil*

(Received 2 June 2011; revised manuscript received 31 July 2011; published 26 September 2011; publisher error corrected 1 March 2012)

The elastic constants of hcp $^4$He are computed using the path-integral Monte Carlo (PIMC) method. The stiffness coefficients are obtained by imposing different distortions to a periodic cell containing 180 atoms, followed by measurement of the elements of the corresponding stress tensor. For this purpose an appropriate path-integral expression for the stress tensor observable is derived and implemented into the PIMC++ package. In addition to allowing the determination of the elastic stiffness constants, this development also opens the way to an explicit atomistic determination of the Peierls stress for dislocation motion using the PIMC technique. A comparison of the results to available experimental data shows an overall good agreement of the density dependence of the elastic constants, with the single exception of $C_{13}$. Additional calculations for the bcc phase, on the other hand, show good agreement for *all* elastic constants.

DOI: 10.1103/PhysRevB.84.094119 PACS number(s): 67.80.B−, 02.70.Ss, 62.20.D−

## I. INTRODUCTION

Despite the intensive research efforts developed over the past six years, the remarkable results of the torsional-oscillator (TO) experiments on solid $^4$He by Kim and Chan[1,2] still elude a consistent explanation. Although it has been suggested that the observed nonclassical rotational inertia (NCRI) is a manifestation of superfluidity in the solid phase,[3–5] several questions remain unanswered. One of them is the apparent correlation between the NCRI data and the observation of elastic stiffening upon cooling, both of which display similar temperature and $^3$He-concentration dependences.[6,7] The observed stiffening effect has been interpreted in terms of dislocation pinning due to $^3$He impurities,[6,8] and this has contributed to ideas that the NCRI may not have an exclusive non-superfluid origin but rather that it might also be a manifestation of mechanical behavior.[8–12]

A major difficulty is the fact that the insight obtained from recent experiments[6,8,13] relies on the indirect interpretation of data, a process that is inevitably based on assumptions. The dislocation-pinning interpretation, for instance, conjectures the presence of dislocation networks that are pinned by $^3$He impurities binding to the dislocation cores.[6,8] Despite the elevated degree of sophistication of recent experiments,[6,8,13] however, it has not yet been possible to verify these assumptions explicitly, hampering a conclusive understanding of the observed phenomenology and its relation to the NCRI data obtained in TO experiments.

In this context, theoretical modeling can serve as a useful complementary approach. In principle, it allows a systematic study of a hierarchy of well-controlled structures not accessible to experiment, starting at the defect-free crystal and progressing through a series of configurations containing different defect geometries. Analysis of the results obtained in these different situations may then assist in the interpretation of existing experimental data or even lead to new predictions. However, a first step in this effort is to gauge the results of these modeling approaches for quantities that can be directly compared to experimental data. In the context of the recent observations of the mechanical behavior of solid $^4$He, its intrinsic elastic properties are an evident target for such an assessment.

The purpose of the present paper is to compare the results of state-of-the-art path-integral Monte Carlo[14,15] (PIMC) calculations based on the Aziz pair potential[16] to the available experimental data for the elastic stiffness constants from the 1970s. The PIMC method has shown to give excellent agreement with experiment for several properties of the liquid and solid states, including the energy, pair correlation functions, structure factors, and superfluid density. Triggered by TO experiments of Kim and Chan, the PIMC methodology has also been applied extensively to the study of $^4$He supersolidity, focusing on a variety of properties, including the possibility of superflow induced by lattice defects such as vacancies,[17,18] and dislocations.[19,20]

The first path-integral approach to the computation of elastic constants was based on a direct measurement of the elastic constants in terms of the second derivatives of the partition function with respect to strain components.[21] Here we adopt a different approach based on the development of an expression for the stress-tensor observable in the path-integral formalism. Not only does this observable allow the determination of the elastic constants of the defect-free crystal, it is also a key observable in the characterization of plastic deformation in terms of lattice defect properties. In this light, this development is of interest in its own right, allowing for instance, an explicit atomistic determination of the Peierls stress for dislocation motion.[22] Here we utilize it to compute the complete set of stress-strain relations by measuring the elastic stress response to small homogeneous deformations, giving the five independent elastic stiffness constants of the hcp $^4$He crystal. In addition to a direct comparison of elastic constants as a function of density, we analyze the degree to which the Cauchy relation, which measures to what extent noncentral forces and zero-point effects are important, is satisfied.

The remainder of the paper has been organized as follows. In Sec. II we derive an expression for the stress-tensor observable within the path-integral formalism based on the pair-action approximation and which has been implemented in the PIMC++ code.[18] Section III describes the employed computational setup and summarizes the parameters used in the simulations. Next, we describe and discuss the obtained results in Sec. IV and summarize in Sec. V.

 

## II. PATH-INTEGRAL EXPRESSION FOR THE STRESS-TENSOR OBSERVABLE

Following the usual approach of Parrinello and Rahman,[23–25] we describe homogeneous distortions of a periodic simulation cell in terms of the box matrix $\mathbb{h}$, whose columns are the three periodic repeat vectors $\boldsymbol{a}$, $\boldsymbol{b}$, and $\boldsymbol{c}$ of the computational cell,[25]

$$\mathbb{h} = \begin{pmatrix} a_x & b_x & c_x \\ a_y & b_y & c_y \\ a_z & b_z & c_z \end{pmatrix}. \tag{1}$$

In terms of the $\mathbb{h}$ matrix, an absolute position $\boldsymbol{r}_i$ within in the cell is written as

$$\boldsymbol{r}_i = \mathbb{h}\, \boldsymbol{s}_i, \tag{2}$$

where $\boldsymbol{s}_i$ is a relative coordinate vector whose components have values ranging between 0 and 1. In this description, homogeneous deformations are described in terms of variations of the $\mathbb{h}$ matrix at fixed relative coordinates $\boldsymbol{s}_i$.

To obtain an expression for the stress tensor in the path-integral formalism we start with its thermodynamic definition, describing its components $\sigma_{ij}$ in terms of derivatives of the appropriate thermodynamic potential. Specifically, we have[25]

$$\sigma_{ij} = -\frac{1}{\det(\mathbb{h})} \sum_{k=1}^{3} \mathbb{h}_{jk} \left( \frac{\partial F}{\partial \mathbb{h}_{ik}} \right)_{N,T}, \tag{3}$$

where

$$F = F(N, \mathbb{h}, T) \tag{4}$$

is the Helmholtz free energy of a system containing $N$ particles that are confined to a volume described by the matrix $\mathbb{h}$ and in thermal equilibrium with a heat bath at temperature $T$. As usual, the microscopic description for the stress tensor is obtained through the connection between the thermodynamic potential and the corresponding partition function. Here, we have

$$F(N, \mathbb{h}, T) = -\frac{1}{\beta} \ln Z(N, \mathbb{h}, T), \tag{5}$$

where $Z(N, \mathbb{h}, T)$ is the canonical partition function and $\beta = (k_B T)^{-1}$. In this manner, the components of the stress tensor $\mathbb{P}$ become

$$\mathbb{P}_{ij} = \frac{1}{\det(\mathbb{h})\beta Z} \sum_{k=1}^{3} \mathbb{h}_{jk} \left( \frac{\partial Z}{\partial \mathbb{h}_{ik}} \right)_{N,T}. \tag{6}$$

In the path-integral formalism, the canonical partition function for a system of distinguishable particles can be written as[14]

$$Z(N, \mathbb{h}, T) = \int \cdots \int dR_0 \cdots dR_{M-1} \times \exp[-S_{\text{path}}(R_0, \cdots, R_{M-1}, R_0)], \tag{7}$$

where $R_k = \{\boldsymbol{r}_{1,k}, \cdots, \boldsymbol{r}_{N,k}\}$ represents the set of position vectors of the $N$ particles in the $k$th time slice of the $M$-bead closed path $R = \{R_0, \cdots, R_{M-1}, R_0\}$, and $S_{\text{path}}(R_0, \cdots, R_{M-1}, R_0)$ is the path action. Proper symmetrization for the case of indistinguishable particles is straightforward.[14]

Describing the position vectors in terms of the $\mathbb{h}$ matrix, the expression becomes

$$Z(N, \mathbb{h}, T) = \int \cdots \int [\det(\mathbb{h})]^{NM} dS_0 \cdots dS_{M-1} \times \exp[-S_{\text{path}}(S_0, \cdots, S_{M-1}, S_0; \mathbb{h})], \tag{8}$$

where $S_k = \{\boldsymbol{s}_{1,k}, \cdots, \boldsymbol{s}_{N,k}\}$ represents the set of scaled position vectors of the $N$ particles in the $k$th time slice. The derivatives of the partition function with respect to the elements of the $\mathbb{h}$ matrix are then given by

$$\frac{\partial Z}{\partial \mathbb{h}_{ij}} = [\det(\mathbb{h})]^{NM} \int \cdots \int dS_0 \cdots dS_{M-1} \times \exp[-S_{\text{path}}] \left[ NM(\mathbb{h}^{-1})_{ji} - \frac{\partial S_{\text{path}}}{\partial \mathbb{h}_{ij}} \right]. \tag{9}$$

Substitution into Eq. (6) then gives

$$\mathbb{P}_{ij} = \frac{1}{\det(\mathbb{h})\beta} \left[ NM\delta_{ij} - \sum_{k=1}^{3} \mathbb{h}_{jk} \left\langle \frac{\partial S_{\text{path}}}{\partial \mathbb{h}_{ik}} \right\rangle \right], \tag{10}$$

where the angular brackets indicate averaging over closed paths. Given that the paths consist of $M$ links, the above expression can also be written in terms of averages over link actions, namely,

$$\mathbb{P}_{ij} = \frac{M}{\det(\mathbb{h})\beta} \left[ N\delta_{ij} - \sum_{k=1}^{3} \mathbb{h}_{jk} \left\langle \frac{\partial S_{\text{link}}}{\partial \mathbb{h}_{ik}} \right\rangle \right]. \tag{11}$$

The hydrostatic pressure $P$ is then given by

$$\mathbb{P} = \frac{1}{3}\text{Tr}\mathbb{P} = \frac{M}{\det(\mathbb{h})\beta} \left[ N - \frac{1}{3} \sum_{i,k=1}^{3} \mathbb{h}_{ik} \left\langle \frac{\partial S_{\text{link}}}{\partial \mathbb{h}_{ik}} \right\rangle \right]. \tag{12}$$

Next we determine the derivative of the link action with respect to the elements of the $\mathbb{h}$ matrix. Here, we are specifically interested in the pair approximation for the action,

$$\begin{aligned} &S_{\text{link}}(R, R'; \tau) \\ &= S_{\text{kin}}(R, R'; \tau) + S_{\text{pot}}(R, R'; \tau) \\ &= \sum_{n=1}^{N} K(\boldsymbol{r}_n, \boldsymbol{r}'_n; \tau) \\ &\quad + \sum_{n<m}^{N} u_2(\boldsymbol{r}_n - \boldsymbol{r}_m, \boldsymbol{r}'_n - \boldsymbol{r}'_m; \tau), \end{aligned} \tag{13}$$

where the first term represents the exact kinetic link action, the second is potential action within the pair-product approximation[14] and $\tau \equiv \beta/M$. It is important to emphasize that, while referred to as the potential action, $u_2$ in fact contains the remainder of the *exact* two-body action (i.e., including both kinetic and potential parts) after separating out the kinetic link action $K$.[14]

The derivatives of interest are then

$$\frac{\partial S_{\text{link}}}{\partial \mathbb{h}_{ij}} = \sum_{n=1}^{N} \frac{\partial K(\boldsymbol{r}_n, \boldsymbol{r}'_n; \tau)}{\partial \mathbb{h}_{ij}} + \sum_{n<m}^{N} \frac{\partial u_2(\boldsymbol{r}_n - \boldsymbol{r}_m, \boldsymbol{r}'_n - \boldsymbol{r}'_m; \tau)}{\partial \mathbb{h}_{ij}}. \tag{14}$$

The kinetic action is given by

$$K(\boldsymbol{r},\boldsymbol{r}';\tau) = \frac{3}{2}\ln(4\pi\lambda\tau) + \frac{|\boldsymbol{r}-\boldsymbol{r}'|^2}{4\lambda\tau}, \tag{15}$$

with $\lambda \equiv \hbar^2/2m$, and is normalized such that

$$\int d\boldsymbol{r}' \exp[-K(\boldsymbol{r},\boldsymbol{r}';\tau)] = 1. \tag{16}$$

To compute the derivatives with respect to the elements of the $\mathbb{h}$ matrix in Eq. (14), we write Eq. (15) in terms of $\mathbb{h}$ and the relative coordinates $\boldsymbol{s}$. The result is

$$K(\boldsymbol{s},\boldsymbol{s}';\mathbb{h},\tau) = \frac{3}{2}\ln(4\pi\lambda\tau) + \ln[\det(\mathbb{h}^{-1})] + \frac{|\mathbb{h}(\boldsymbol{s}-\boldsymbol{s}')|^2}{4\lambda\tau}, \tag{17}$$

which is normalized such that

$$\int d\boldsymbol{s}' \exp[-K(\boldsymbol{s},\boldsymbol{s}';\mathbb{h},\tau)] = 1. \tag{18}$$

The derivatives with respect to the $\mathbb{h}$-matrix elements are then given by

$$\frac{\partial K(\boldsymbol{s},\boldsymbol{s}';\mathbb{h},\tau)}{\partial \mathbb{h}_{ij}} = -\mathbb{h}_{ji}(\mathbb{h}^{-1})_{ii}(\mathbb{h}^{-1})_{jj} + \frac{1}{2\lambda\tau}\sum_{k=1}^{3}\mathbb{h}_{ik}(\boldsymbol{s}-\boldsymbol{s}')_k(\boldsymbol{s}-\boldsymbol{s}')_j, \tag{19}$$

where the subscripts on the relative-position difference vectors refer to their respective Cartesian components.

The derivatives with respect to the potential action are obtained in a similar manner, writing the function $u_2(\boldsymbol{r},\boldsymbol{r}';\tau)$ in Eq. (13) in terms of the matrix $\mathbb{h}$ and the relative coordinates $\boldsymbol{s}$ and $\boldsymbol{s}'$. In practice, it is useful[26] to express $u_2$ in terms of a different coordinate set. Defining

$$q \equiv \tfrac{1}{2}(|\boldsymbol{r}| + |\boldsymbol{r}'|) = \tfrac{1}{2}(|\mathbb{h}\boldsymbol{s}| + |\mathbb{h}\boldsymbol{s}'|), \tag{20}$$

$$z \equiv |\boldsymbol{r}| - |\boldsymbol{r}'| = |\mathbb{h}\boldsymbol{s}| - |\mathbb{h}\boldsymbol{s}'|, \tag{21}$$

$$t \equiv |\boldsymbol{r}-\boldsymbol{r}'| = |\mathbb{h}(\boldsymbol{r}-\boldsymbol{r}')|, \tag{22}$$

the potential action then takes the form

$$S_{\rm pot} = \sum_{n<m}^{N} u_2(q_{mn},z_{mn},t_{mn};\tau), \tag{23}$$

where, for instance,

$$q_{mn} = \tfrac{1}{2}(|\mathbb{h}(\boldsymbol{s}_n-\boldsymbol{s}_m)| + |\mathbb{h}(\boldsymbol{s}'_n-\boldsymbol{s}'_m)|). \tag{24}$$

The derivatives with respect to the $\mathbb{h}$-matrix elements are then given by

$$\frac{\partial u_2(q,z,t;\tau)}{\partial \mathbb{h}_{ij}} = \left(\frac{\partial q}{\partial \mathbb{h}_{ij}}\frac{\partial u_2}{\partial q} + \frac{\partial z}{\partial \mathbb{h}_{ij}}\frac{\partial u_2}{\partial z} + \frac{\partial t}{\partial \mathbb{h}_{ij}}\frac{\partial u_2}{\partial t}\right) \tag{25}$$

with

$$\frac{\partial q}{\partial \mathbb{h}_{ij}} = \frac{1}{2}\left(\frac{\sum_k \mathbb{h}_{ik}s_k s_j}{|\mathbb{h}\boldsymbol{s}|} + \frac{\sum_k \mathbb{h}_{ik}s'_k s'_j}{|\mathbb{h}\boldsymbol{s}'|}\right), \tag{26}$$

$$\frac{\partial z}{\partial \mathbb{h}_{ij}} = \left(\frac{\sum_k \mathbb{h}_{ik}s_k s_j}{|\mathbb{h}\boldsymbol{s}|} - \frac{\sum_k \mathbb{h}_{ik}s'_k s'_j}{|\mathbb{h}\boldsymbol{s}'|}\right), \tag{27}$$

and

$$\frac{\partial t}{\partial \mathbb{h}_{ij}} = \left(\frac{\sum_k \mathbb{h}_{ik}(\boldsymbol{s}-\boldsymbol{s}')_k(\boldsymbol{s}-\boldsymbol{s}')_j}{|\mathbb{h}(\boldsymbol{s}-\boldsymbol{s}')|}\right). \tag{28}$$

The calculation of the stress tensor is then based on using expressions (19) and (25) in Eqs. (11) and (14).

## III. COMPUTATIONAL DETAILS

All calculations are based on an orthorhombic computational cell containing 180 $^4$He atoms arranged on a hcp lattice characterized by the ideal ratio $c/a = 1.633$, which is within 0.3% of the experimental estimates for all considered densities.[27] The cell is constructed in such a manner that the $x$, $y$, and $z$ axes are parallel to the crystallographic $[\bar{1}\,2\,\bar{1}\,0]$, $[\bar{1}\,0\,1\,0]$, and $[0\,0\,0\,1]$ directions, respectively. Standard periodic boundary conditions are applied throughout. The simulations have been carried out using the PIMC++ package,[18] which is a C++ implementation of the PIMC algorithms described in Ref. 14. The used pair action was obtained from a standard matrix squaring procedure[14,15] using the Aziz HFD-B3-FCI1 pair potential[16] and an interaction cutoff of 8 Å. All PIMC simulations employ a time step $\tau \equiv \beta/M = 1/40$ K$^{-1}$,[28] with $\beta$ the inverse temperature and $M$ the number of beads in the ring polymers.

The determination of the elastic stiffness constants $C_{ijkl}$ is based on the definition[29]

$$\sigma_{ij} = \sum_{k,l} C_{ijkl}\epsilon_{kl}, \tag{29}$$

where $\epsilon_{kl}$ is the $kl$ component of the strain tensor and $\sigma_{ij}$ is the $ij$ component of the corresponding stress tensor. The stiffness constants are then determined by imposing different kinds of strains $\epsilon_{kl}$ and measuring the induced stress responses $\sigma_{ij}$. Specifically, each simulation is carried out using a cell in which only one of the six independent strain components (measured with respect to the undeformed cell reference) is different from zero. In this manner, there is only one term in the summation of Eq. (29). Exploring the linearity of Eq. (29), we determine the stress response as a function of the magnitude of a given strain component. The stiffness constants are then given by the slopes of the $\sigma_{ij}(\epsilon_{kl})$ graphs,

$$C_{ijkl} = \frac{d\sigma_{ij}}{d\epsilon_{kl}}. \tag{30}$$

## IV. RESULTS AND DISCUSSION

Figure 1 shows typical results for the stress components as a function of the imposed strain at a temperature of 1 K and a molar volume of 20 cm$^3$. Figure 1(a) shows the shear stress response $\sigma_{xz}$ as a function of the imposed shear strain $\epsilon_{xz}$, where the indications $x$ and $z$ refer to the $x$ and $z$ directions of the computational cell. In all cases, we verified that the small distortions did not cause any disruptions of the crystal structure, leading only to small homogeneous deformations of the hexagonal structure within the elastic limit. The behavior is distinctly linear up to absolute strain values of 2%, as attested by the linear fit shown by the full line. As expected, the line passes through the origin, with no shear stress being present at

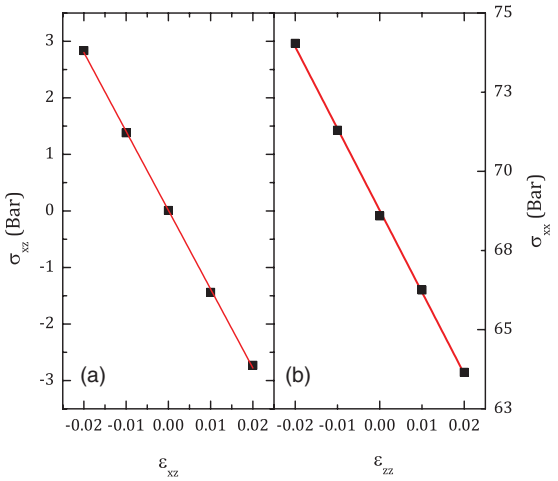


FIG. 1. (Color online) Stress response as a function of imposed deformation. Magnitude of the error bars corresponds to size of symbols. Full lines depict linear fits to the PIMC results. (a) Shear stress $\sigma_{xz}$ in response to shear strain $\epsilon_{xz}$, scale of the left-hand side. (b) Tensile stress $\sigma_{xx}$ a function of tensile strain $\epsilon_{zz}$, scale of the right-hand side.

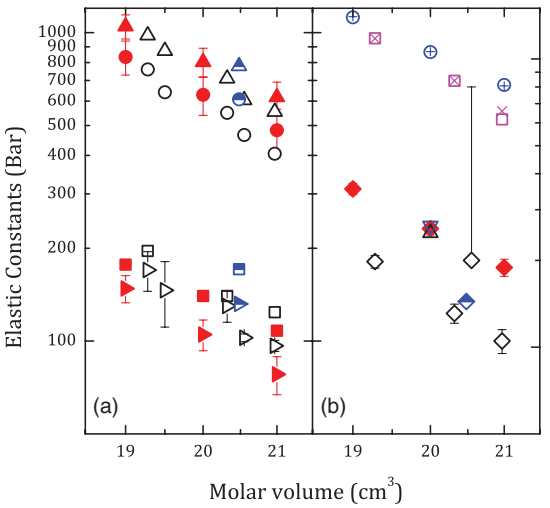


FIG. 2. (Color online) Elastic constants and some of their specific combinations for hcp solid $^4$He as a function of the molar volume at a temperature of 1 K. (a) Filled symbols depict PIMC results. Half-filled symbols represent zero-temperature VMC results of Ref. 22. Open symbols represent corresponding experimental data. When error bars are not shown they are smaller than the symbol size. $C_{33}$ (upward triangles), $C_{11}$ (circles), $C_{44}$ (squares), $C_{66}$ (right triangles). (b) $C_{13}$ PIMC (filled diamonds, $\tau = 1/40\ K^{-1}$, open upward triangle, $\tau = 1/80\ K^{-1}$, open downward triangle, result obtained from bulk modulus), $C_{13}$ experimental (open diamonds), $C_{13}$ VMC (half-filled diamond), $C_{11} + C_{12}$ PIMC (○), $C_{33} + C_{13}$ PIMC (pluses), $C_{11} + C_{12}$ experimental (squares), $C_{33} + C_{13}$ experimental (crosses).

zero shear deformation. The slope of the line then determines the shear elastic constant $C_{xzxz}$ or, in Voigt notation,[29] $C_{44}$, usually known as the shear modulus $\mu$. Figure 1(b) shows a similar response curve, plotting the tensile stress $\sigma_{xx}$ in response to the tensile strain $\epsilon_{zz}$. In this case the stress response does not pass through the origin given that the reference cell is in a state of hydrostatic compression. Once again the behavior is manifestly linear, with the slope giving the value of the elastic constant $C_{xxzz}$ or, in Voigt notation, $C_{13}$.

Using stress-strain curves of the type shown in Fig. 1 obtained from the PIMC simulations, we determine the $6 \times 6$ elastic-constant matrix[29] of hcp solid $^4$He as a function of the molar volume at a temperature of 1 K. As expected, the results are found to obey the symmetry relations for hexagonal crystals,[29] leaving only five independent stiffness constants. These are shown in Fig. 2, which also includes sets of experimental data produced in the 1970s.[30–35] A comparison between the theoretical and experimental data, however, must be conducted with some care. Whereas the PIMC calculations give values for the *isothermal* stiffness constants, the ultrasonic experimental data typically probe the *adiabatic* elastic constants. Accordingly, a direct comparison between the two data sets is meaningful only if the difference between these two kinds of elastic constants is small. In its estimation, we applied the expressions for the difference between the isothermal and adiabatic elastic constants[36] and used experimental thermodynamic data[37] for the isochoric heat capacity $C_v$ and the isochoric pressure coefficient $(\partial P/\partial T)_v$. For a molar volume of 19.135 cm$^3$ and a temperature of 1K, we find the difference to be of the order of $10^{-1}$ bar, which is very small compared to the absolute values of the elastic constants and their error bars, thus justifying a direct comparison of the PIMC data with experiment.

Figure 2(a) compares our PIMC results to experimental data for the four elastic constants $C_{33}$, $C_{11}$, $C_{44}$, and $C_{66}$. For further comparison we have also included results from recent variational Monte Carlo (VMC) for $T = 0\ K$ based on the shadow wave function formalism.[22] The agreement between PIMC and experiment is excellent for $C_{33}$ and $C_{11}$, with values essentially within each others error bars across the considered density range. The agreement is also good for $C_{44}$ and $C_{66}$, with the PIMC values ∼10–20% below the experimental data. For these four constants, the PIMC results also show slightly better agreement with experiment compared to the VMC data, which systematically overestimate all four constants by ∼20–30%.

The situation is markedly different for the remaining independent elastic constant, $C_{13}$, however. As shown by the diamond symbols in Fig. 2(b) the PIMC data overestimate experiment by 50–100%, with exception of the data point measured by Greywall in 1971, although the latter is characterized by an error bar of 300%.[32] To further verify our result we performed additional computations at a molar volume of 20 cm$^3$. First, we carried out the PIMC calculations using a reduced time step of $\tau = 1/80\ K^{-1}$. Furthermore, we also determined $C_{13}$ in an indirect way, computing the bulk modulus $B = -V(\partial P/\partial V)_T$ by a finite-difference derivative of the hydrostatic pressure with respect to volume changes and using the relation $C_{13} = \frac{1}{2}(3B - C_{33})$. As can be seen in Fig. 2(b), neither led to significantly different results for $C_{13}$, lending further support to the internal consistency of our calculations. Interestingly, the VMC result for $C_{13}$ is actually in good agreement with experiment, differing by ∼10%.

To investigate the origin of this discrepancy, it is useful to verify whether certain relations, different from those

associated with the crystal symmetry, hold. One of these is the relation

$$C_{11} + C_{12} = C_{33} + C_{13}, \tag{31}$$

which should be satisfied in case the $c/a$ ratio is independent of the density. This independence has been verified experimentally for a wide range of pressure values.[30] This is consistent with the fact that the experimental values of the left- and right-hand sides of Eq. (31) are essentially equal, as shown by the open squares and crosses, respectively, in Fig. 2(b). Despite the overestimate for stiffness constant $C_{13}$, the PIMC results are in fact consistent with this characteristic of solid $^4$He in the hcp phase as shown by the open circles and pluses in the same plot.

Another concerns the validity of the so-called Cauchy relation,[38,39] $C_{13} - P = C_{44} + P$, where $P$ is the applied hydrostatic pressure. These are relations between elastic constants that are expected to hold when the (a) interatomic interactions can be described by purely two-body central forces and (b) when vibrational effects, zero-point or thermal in origin, are negligible. It is useful to quantify deviations from this relation through the parameter[35,39]

$$\delta = \frac{C_{44} + P - (C_{13} - P)}{(C_{13} - P)}. \tag{32}$$

For a classical crystal at $T = 0$ K and characterized by pairwise central interaction forces one has $\delta = 0$. Deviations from this value are then a measure of the magnitude of vibrational effects and the importance of many-body interaction forces. In the case of quantum crystals at low temperatures, the deviation thus is a probe for the role of zero-point motion and/or many-body interactions. It seems plausible, however, that the latter are rather small for the condensed phases of $^4$He.[40]

Figure 3 shows $\delta$ as a function of the density for the experimental data and our PIMC results for the hcp phase. The results show a distinct discrepancy. While the calculations give relatively small deviation values, ranging between 0.05 and 0.14, the experimental deviations are 0.8–0.9. Again, this discrepancy can be traced back to the difference in the value of stiffness constant $C_{13}$.

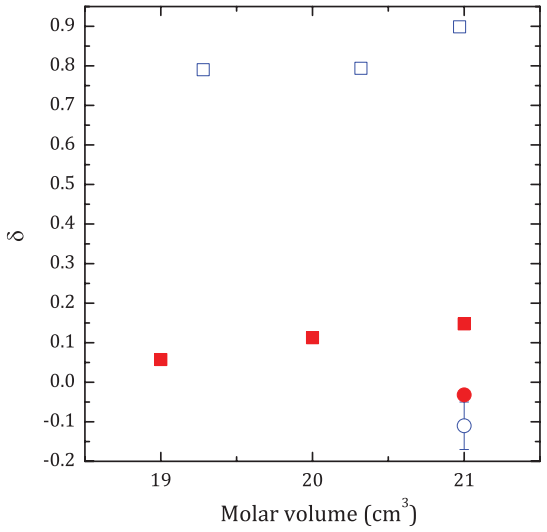


FIG. 3. (Color online) Cauchy deviation values for the hcp (squares) and bcc (circles) phases. Experimental results (open symbols), PIMC results (full symbols).

To further assess these issues we also computed the elastic constants for the bcc phase, which exists at similar densities and temperatures as those considered for the hcp form. In this case, we find very good agreement between PIMC and experiment for *all* elastic constants. Specifically, at a density of 21 cm$^3$ and a temperature of 1.5 $K$, the PIMC calculations give $C_{11} = 371 \pm 43$, $C_{12} = 330 \pm 25$, and $C_{44} = 217 \pm 4$ bar. Inelastic neutron scattering measurements, on the other hand, give $C_{11} = 349 \pm 15$, $C_{12} = 301 \pm 10$, and $C_{44} = 215 \pm 8$ bar so that the differences between PIMC and experiment are less than 10% for all stiffness constants. As a result, there are no significant discrepancies between PIMC and experimental Cauchy deviations, as can be gauged by the parameter $\delta = (C_{44} - C_{12} + 2P)/(C_{12} - P)$ in Fig. 3.

The interpretation of the above results is challenging. In the present situation, our results agree very well with experiment for four of the five independent elastic moduli of the hcp phase, but show a deviation for the remaining constant, $C_{13}$. If this were to be interpreted as a flaw in our calculations, then discrepancies would also be expected for other phases. This does not seem to be the case. In addition to previous results for the liquid phase based on very similar interaction models,[14] our calculations are in very good agreement with experiment for *all* elastic constants of the bcc phase. A further element in this discussion is that, although conducted for zero temperature, recent VMC and diffusion Monte Carlo results[22,41] do not seem to show this deviation for $C_{13}$ in hcp $^4$He.

To unveil this puzzle it would be extremely useful to renew the experimental data for the elastic constants of hcp $^4$He. The data sets available today are more than 30 years old and, with present experimental capabilities, it should be possible to obtain the elastic constants with significantly greater accuracy. Not only would such data be useful toward gauging current theoretical modeling approaches, they would also be particularly useful, for instance, in understanding the elastic properties of polycrystalline $^4$He samples.[11] In addition, such information would also be of value in discriminating between changes in elasticity and supersolidity, respectively, when interpreting frequency changes in TO experiments.[11]

## V. CONCLUSIONS

In summary, in this paper we have reported values of the elastic stiffness constants of solid $^4$He in the hcp phase determined using the PIMC approach based on the Aziz pair-potential model. To this end we have developed an expression for the stress observable in the path-integral formalism, allowing the direct measurement of the internal stress state of a system in PIMC simulations. This development is of interest in its own right, allowing for instance, an explicit atomistic determination of the Peierls stress for dislocation motion.[22] Here, we use it to compute the elastic stiffness constants by measuring the linear stress response to imposed small strain conditions.

Four of the five computed elastic stiffness constants as a function of density show good agreement with experiment. The stiffness coefficient $C_{13}$, which is 50–100%

larger than reported experimental values, is an exception. This discrepancy leads to very different deviations in the Cauchy relation associated with $C_{44}$ and $C_{13}$. The same calculations for the bcc phase, on the other hand, show good agreement between experiment and PIMC for all elastic constants.

**ACKNOWLEDGMENTS**

We gratefully acknowledge support from the Brazilian agencies CNPq, Fapesp, and Capes. We thank Prof. J. Beamish for helpful discussions. The calculations were performed at CCJDR-IFGW-UNICAMP and CENAPAD-SP.

*Corresponding author: dekoning@ifi.unicamp.br

[1] E. Kim and M. H. W. Chan, Nature (London) **427**, 225 (2004).
[2] E. Kim and M. H. W. Chan, Science **305**, 1941 (2004).
[3] A. J. Leggett, Phys. Rev. Lett. **25**, 1543 (1970).
[4] G. V. Chester, Phys. Rev. A **2**, 256 (1970).
[5] S. Balibar, Contemp. Phys. **48**, 31 (2007).
[6] J. Day and J. Beamish, Nature (London) **450**, 853 (2007).
[7] M. H. W. Chan, Science **319**, 1207 (2008).
[8] X. Rojas, A. Haziot, V. Bapst, S. Balibar, and H. J. Maris, Phys. Rev. Lett. **105**, 145302 (2010).
[9] J. D. Reppy, Phys. Rev. Lett. **104**, 255301 (2010).
[10] J. Beamish, Physics **3**, 51 (2010).
[11] H. Maris and S. Balibar, J. Low Temp. Phys. **160**, 5 (2010).
[12] H. Maris and S. Balibar, J. Low Temp. Phys. **162**, 12 (2011).
[13] J. Day, O. Syshchenko, and J. Beamish, Phys. Rev. B **79**, 214524 (2009).
[14] D. M. Ceperley, Rev. Mod. Phys. **67**, 279 (1995).
[15] W. Krauth, *Statistical Mechanics: Algorithms and Computations* (Oxford University Press, Oxford, 2006).
[16] R. A. Aziz, A. R. Janzen, and M. R. Moldover, Phys. Rev. Lett. **74**, 1586 (1995).
[17] M. Boninsegni, A. B. Kuklov, L. Pollet, N. V. Prokof'ev, B. V. Svistunov, and M. Troyer, Phys. Rev. Lett. **97**, 080401 (2006).
[18] B. K. Clark and D. M. Ceperley, Comput. Phys. Commun. **179**, 82 (2008).
[19] M. Boninsegni, A. B. Kuklov, L. Pollet, N. V. Prokof'ev, B. V. Svistunov, and M. Troyer, Phys. Rev. Lett. **99**, 035301 (2007).
[20] S. G. Söyler, A. B. Kuklov, L. Pollet, N. V. Prokof'ev, and B. V. Svistunov, Phys. Rev. Lett. **103**, 175301 (2009).
[21] P. Schöffel and M. H. Müser, Phys. Rev. B **63**, 224108 (2001).
[22] R. Pessoa, S. A. Vitiello, and M. de Koning, Phys. Rev. Lett. **104**, 085301 (2010).
[23] M. Parrinello and A. Rahman, J. Appl. Phys. **52**, 7182 (1981).
[24] M. Parrinello and A. Rahman, J. Chem. Phys. **76**, 2662 (1982).
[25] M. E. Tuckerman, *Statistical Mechanics: Theory and Molecular Simulation* (Oxford University Press, Oxford, 2010).
[26] K. P. Essler, "Advancements in the Path Integral Monte Carlo Method for Many-body Quantum Systems at Finite Temperature," Ph.D. thesis, University of Illinois at Urbana-Champaign (2006).
[27] Y. A. Freiman, S. M. Tretyak, A. Grechnev, A. F. Goncharov, J. S. Tse, D. Errandonea, H.-k. Mao, and R. J. Hemley, Phys. Rev. B **80**, 094112 (2009).
[28] B. Bernu and D. Ceperley, in *Quantum Simulations of Complex Many-Body Systems: From Theory to Algorithms*, NIC Series, Vol. 10, edited by A. M. J. Grotendorst and D. Marx (John von Neumann Institute for Computing, Jülich, 2002), p. 51.
[29] J. F. Nye, *Physical Properties of Crystals: Their Representation by Tensors and Matrices* (Oxford University Press, Oxford, 1985).
[30] J. P. Franck and R. Wanner, Phys. Rev. Lett. **25**, 345 (1970).
[31] R. H. Crepeau, O. Heybey, D. M. Lee, and S. A. Strauss, Phys. Rev. A **3**, 1162 (1971).
[32] D. S. Greywall, Phys. Rev. A **3**, 2106 (1971).
[33] R. Wanner and J. P. Franck, Phys. Rev. Lett. **24**, 365 (1970).
[34] D. S. Greywall, Phys. Rev. B **16**, 5127 (1977).
[35] J. Beamish, in *Handbook of Elastic Properties of Solids, Liquids, and Gases*, Vol. 2, edited by M. Levy and L. Furr (Academic Press, San Diego, 2000).
[36] D. C. Wallace, *Thermodynamics of Crystals* (Dover Publications, New York, 1998), p. 26.
[37] G. Ahlers, Phys. Rev. A **2**, 1505 (1970).
[38] M. Born and K. Huang, *Dynamical Theory of Crystal Lattices* (Clarendon, Oxford, 1954).
[39] C.-S. Zha, H.-k. Mao, and R. J. Hemley, Phys. Rev. B **70**, 174107 (2004).
[40] S. Ujevic and S. A. Vitiello, J. Chem. Phys. **119**, 8482 (2003).
[41] C. Cazorla, Y. Lutsyshyn, and J. Boronat, e-print arXiv:1106.1520 (2011).